Austin Environmental Sciences

Open Access

Austin Publishing Group

Special Article: Thorium Fuel Production

Speciation of Iodide and Iodate Anions in Geochemical Environments: A Theory Driven Experimental Study

Mahesh Sundararajan[1,2*]; Jayshree Ramkumar[2,3]; Arulkumar Rasu[4]; Ponnambalam Venuvanalingam[4]

[1]Theoretical Chemistry Section, Chemistry Division, Bhabha Atomic Research Centre, India

[2]HomiBhabha National Institute, India

[3]Analytical Chemistry Division, Bhabha Atomic Research Centre, India

[4]Theoretical and Computational Chemistry Laboratory, School of Chemistry, Bharathidasan University, India

[*]Corresponding author: **Mahesh Sundararajan**
Theoretical Chemistry Section, Chemistry Division, Bhabha Atomic Research Centre, Mumbai, India
Tel: +91-22-25595607
Email: smahesh@barc.gov.in

Received: July 31, 2023
Accepted: September 09, 2023
Published: September 16, 2023

Abstract

Speciation of heavy metal ions in geochemical environment is utmost importance due to its environmental relevance. Iodine exists as iodide and iodate anions and are heavier anions, and they can be more labile in the absence of humic environments. This study particularly focusses on iodine speciation in Humic Acid (HA) environments. First, we have carried out extensive quantum chemical calculations to understand the structure-function relationship of iodide and iodate binding in humic acids. We predict that iodide anion binds through hydrogen bonding and are thus weak in acidic conditions. Iodate anion binds at the macrocyclic pocket of the humic acid, and is somewhat pH independent. Computed structure of the complex and binding energies explain the binding affinities of iodide and iodate with HA and quantum theory of atoms and molecules QTAIM analysis reveal the nature of forces involved in each case. To justify our computational claim, sorption experimental studies are carried out on the uptake of iodine species with humic acid. The studies are quite encouraging and there is a close agreement between the theoretical and experimental results.

Introduction

With diminishing fossil fuel resources, it is vital to increase the energy production to serve the growing population. Significant advances in nuclear technologies make nuclear power a viable solution to the ongoing energy demands. Nuclear energy is advantageous in several means such as well-established technology, harnessing maximum energy through efficient reprocessing and little waste being generated [1]. On the other hand, nuclear accidents are dangerous and can release several toxic, radioactive and hazardous nuclear waste that can be detrimental to the environment. In the last five decades, only two major nuclear accidents with INES level of 7 have occurred namely Chernobyl in 1986 and Fukushima in 2011 [2]. In both accidents, significant amount of radioactive materials such as Sr^{90}, Cs^{137} and I^{131} were released in the environment [3,4]. Radionuclide iodine, I^{131}, with the half-life of 8 days is one of the hazardous wastes of fuel reprocessing plant which get released to the environment during normal plant operation [5]. Due to its lower half life, it is less important in biological point of view. On the other hand, I^{129} (half-life = 1.57×10^{7}yrs) is a radionuclide of interest for disposal of high level waste produced by nuclear fuel reprocessing plant and also found in the seawater offshore Fukushima [6,7]. On the other hand, radioiodine is indeed administered in nuclear medicine such as hyperthyroidism [8].

Though heavy ion, iodine species can be dispersed through air and can be found in different environments such as those reported in Antarctica and can contaminate the natural habitat [9]. The oxidation state of iodine varies from –1 to +7 and thus it exists in various forms in nature at different pHs after getting released to the environment. The main chemical forms of iodine are iodide (I^-), iodate (IO_3^-) and molecular iodine (I_2) and it may also exist in organic iodine form (CH_3I). Besides this, iodine is an essential micronutrient for the production of thyroid hormones in animals and humans. Radioactive iodine is concentrated in the thyroid gland can lead to the direct threat to human populations [10].

Natural Organic Matter (NOM) such as Humic (HA) and Fulvic Acids (FA) are known to bind several ions including radionuclides such as uranyl, Cs^+, Sr^{2+} and iodide ions [11-15]. With less oxygen content, HAs are more hydrophobic than FA, there by binds bulky iodine species better through favorable van der Waals interactions. Due to the availability of deprotonated Lewis basic sites, FA binds cationic species strongly in neutral to alkaline pH medium. It is for these reasons, the mobility of Sr^{2+} and uranyl ion are controlled by NOM environment, whereas the bulky Cs^+ ion is more mobile with varying water concentration even in the presence of NOM environment [12].

Citation: Sundararajan M, Ramkumar J, Rasu A, Venuvanalingam P. Speciation of Iodide and Iodate Anions in Geochemical Environments: A Theory Driven Experimental Study. Austin Environ Sci. 2023; 8(3): 1093.

Stable iodine I^{127} and I^{129} are major bi-product of nuclear fission and undergoes complex geochemical cycling in the environment. Only handful reports are available on the speciation of iodine species with NOM is available [16-18]. In this paper, we have carried out detailed Density Functional Theory (DFT) calculations on the structures and binding modes and affinities of iodide and iodate anions in HA. The computed geometries and energetics could easily explain the interesting results obtained from the sorption experiments of iodide and iodate with humic acid as sorbent.

Experimental Details

Choice of Models

We have taken the Stevenson's model for HA that satisfies several structural requirements. The model consists of several functional groups such as aromatic hydroxo, quinone, sugar, aromatic carboxylic acid and amino acids such as tyrosine that are key moieties present in HA revealed by several spectroscopic techniques. We have used this model earlier to understand the speciation of uranyl in HA environments [12]. With unknown X-ray structures, we have carried out extensive multi-scale model simulations to derive a reasonable structure that is used to understand the speciation of heavy metal ions.

Computational Calculations

Both geometry optimizations and vibrational frequency computations were carried out using Density Functional Theory (DFT) [19]. DFT calculations were carried out as implemented in the TURBOMOLE 7.2 version of *ab initio* quantum chemistry program [20]. Geometry optimizations were performed with BP86 functional [21,22,33] including Grimme's D3 dispersion correction [23] with Becke-Johnson damping factor (D3-BJ) [24]. All atoms except I are represented using the *def2*- SV (P) basis set [25]. For I, a *def2*-SV (P) basis set and small core pseudopotential (Z=28) for core electrons is used. The calculations are accelerated using a Resolution of Identity (RI) approximation by incorporating the corresponding auxiliary basis set. Analytical vibrational frequencies within the harmonic approximation were computed with the abovementioned basis sets to confirm proper convergence to well-defined minima. Standard approximation was used to obtain zero-point vibrational energy and entropy corrections. We obtained solvation energies using the optimized gas-phase structures from the COSMO solvation model with dielectric constant ε=80 (water) using the default radii. Single point calculations were carried out with M06 functional with def2-TZVP basis set for all atoms with *def2*-ECP for I. We have earlier used this computational strategy for several systems and their agreement with experiments have been satisfactory [26,27]. Chimera 1.12c software [28] is used to plot the molecular orbitals (iso value of 0.04).

In addition, Quantum Theory of Atoms In Molecules (QTAIM) assessment of topologies of the electron density in weak bonds holding the host and guest is used to better understand the current bonding situation in HA complexes [29,30]. Based on Bader's theory, QTAIM analysis describes the bonding region between atoms in terms of topological characteristics of the electron density (ρ(r)) and Laplacian of the electron density ($\nabla^2\rho(r)$). For instance, the Bond Critical Bond (BCP), which is represented as a (3,-1) critical point in the QTAIM topography, denotes a chemical bond between two atoms, while a (3,+1) critical point (RCP) denotes a ring structure in a molecular system. Particularly, ρ(r) values at the BCPs can be connected to bond strength. Hybrid B3LYP functional [21,22,31] with the dispersion correction D3(BJ) has been used to perform QTAIM calculations. BP86-D3(BJ)/*def2*-SV(P) optimized geometries are used to create primary wave function file for AIM calculations. *def2*-SVP basis set is used for all atoms. B3LYP- D3(BJ)/*def2*-SVP energy gradients are calculated using the nuclear coordinates generated at BP86-D3(BJ)/*def2*-SVP level during the single point calculations using "FORCE" keyword. We have used QTAIM calculations to understand the nature of weak interactions in several studies [32-34].

Experimental Setup

The sorption studies were carried out in batch mode [35]. A known concentration of pure solution of iodide / iodate (5ppm), maintained at different pH values between 1.0-4.0, was contacted with approximately 0.05g of humic acid for a fixed time of 30 mins. At the end of equilibration time, the solid was completely removed by centrifugation and the amount of iodide / iodate left in solution was analyzed spectrophotometrically using methylene blue [36]. From these data, the amount taken up (%) was calculated.

Results and Discussion

Geometric Structures of Iodine Species and HA

We have taken solvated iodide and iodate as possible species of iodine studied here. The optimized species are shown in Figure 1. Unlike chloride and bromide anions, the solvated structure of iodide is somewhat different [32]. The solvated structure of iodide is partially exposed to vacuum due to its bulky nature of anions. This is not unexpected as for bulky ions such as iodide a similar trend is also noted for alkali metal ions such as the solvated structure of Cs^+ ions [37,38]. For iodate anion, a planar structure is noted. The major difference between the iodide and iodates are the charges carried on the iodine moiety due to the differing oxidation state of the species investigated here. In iodide, the oxidiation state of iodine is –I that carries partial negative charge, whereas for iodate anion, the oxidation of iodine is +VII and thus carries a partial positive charge. These variations can lead to the different binding modes with HA.

We have optimized the structure of HA (Figure 2a) and the results reveal several interesting geometric features. We note the HA has two distinct geometric arrangement denoted as *'head' and 'tail'* part (Figure 2b and 2c) respectively. The catechol and other organic fragments of HA are involved in hydrogen bonding with the tyrosine amino acid forming a macrocyclic type head portion that can accommodate guests of suitable size. The tail portion can bind guest molecules through favorable electrostatic interactions with the aromatic carboxylic acids. Partially solvated uranyl and Sr^{2+}cations preferably bind through the carboxylates and through the hydroxyl part of the HA [12]. We have explored the binding of iodide and iodate in both the head and tail portion of HA.

Binding of Iodide anion to HA

Being a bulky highly polarizable ion, iodide can bind in two different binding pockets that are carefully chosen denoted as HA_I_1 and HA_I_2. The optimized structures are shown in Figure 3. A careful look at the geometric feature of HA_I_1 clearly indicates two different hydrogen bonding interactions are present between the HA and iodide anion. There exist a hydrogen bonding between the HA and iodide anion by 2.4 Å, whereas two hydrogen bonding interactions are present

between the water molecules and the iodide anion by 2.8 Å.

In the second structure, the solvated iodide anion is encapsulated inside the head portion of HA denoted as HA_I_2. We note four to five strongly hydrogen bonded interactions of phenolic and catechol functional groups and water molecules with iodide anion by 2.6 Å. In additionto this, we find several anion-π interactions between the aromatic phenyl rings with iodide ion by 3.5 Å. We have quantified the strength of these interactions through AIM calculations (*vide infra*). Between the two structures, HA_I_2 is the most stable structure whose binding energy is computed to be –2.3 kcal/mol, whereas unfavorable binding is noted for HA_I_1. These variations clearly suggest that additional hydrophobic interactions dictate the binding of bulky iodide to HA.

Binding of Iodate to HA

The iodide binding takes place through hydrogen bonding between the protons of HA to iodide anion, whereas in iodate, it is the oxygen atoms ligated to the hepta-valent iodate interacting with the protons of HA. Similar to iodide, we have explored two different binding site of iodateto HA denoted as HA_IO_3_1 and HA_IO_3_2 in Figure 4. The iodate binding at the peripheral region is interacting strongly through favorable hydrogen bonding with 1.4 Å. In HA_IO_3_2 species, a number of hydrogen bonding interactions are found between the iodate and HA moieties in less than 2.0 Å. In addition to this, several non-covalent interactions are noticed from AIM calculations (*vide infra*). The binding affinity for iodate with HA is –108.5 kcal/mol that indicates that the binding is stronger compared to binding with iodide anion.

QTAIM Analysis

We have carried out QTAIM electron density calculations to understand the nature of weak interactions present in HA_I_2 and HA_IO_3_2 species. These two species are chosen due to their favorable binding energies for iodide and iodate at the head portion of HA is discussed inhere, whereas for the other two species, HA_I_1 and HA_IO_3_1, the results are shown in ESI. QTAIM electron density ρ(r) at the BCP is typically substantial (>0.2 a.u.) and has a negative $\nabla^2\rho(r)$ for covalent (shared shell) interactions. On the other hand, ρ(r) is modest (0.10 a.u.) and $\nabla^2\rho(r)$ is positive for ionic, van der Waals, or hydrogen bond (closed shell) interactions. In Table1 and Table S1, we have shown that topological characteristics at the BCPs between HA and iodide/iodate and their molecular graph is given in Figure S1-S4. Only significant interactions that have considerable bond strengths are considered for discussion.

Based on the bond paths and associated BCPs, several non-covalent interactions are identified. In HA_I_2 species, the stabilization of [I^- $(H_2O)_2$] in HA is due to thirteen non- bonding interactions as shown in molecular graph (Figure S1). As discussed above, solvated I^- is stabilized by forming intramolecular hydrogen bonds from each water molecule. Hydrogen bonds are more predominant than halogen bonding. Five intermolecular hydrogen bonds are observed in which I^- bound water molecule forms the strong H-bond (1.87 Å) with oxygen in quinone group of HA. Therefore this hydrogen-bond has higher ρ(r) (0.0307 a.u.) than others. Other weak interactions are also found as shown in Table 1.

In HA_IO_3_2 host-guest complex, eight strong non-bonding interactions are found as shown in Table 1 (Figure S3). Four intermolecular hydrogen bonds are observed and these interactions favor the binding of IO_3 in HA in which iodate bound oxygen atoms makes strong hydrogen bonds with aromatic di-hydroxo (1.43Å) and hydroxo (1.49Å) group present in HA. Therefore these two H-bonds have higher ρ(r) (>0.07 a.u.) than others. The contour plot of $\nabla^2\rho(r)$ of these interaction is shown in Figure 5. Other weak interactions such as O···I, C···I and C···O also involved as shown in the Table 1.

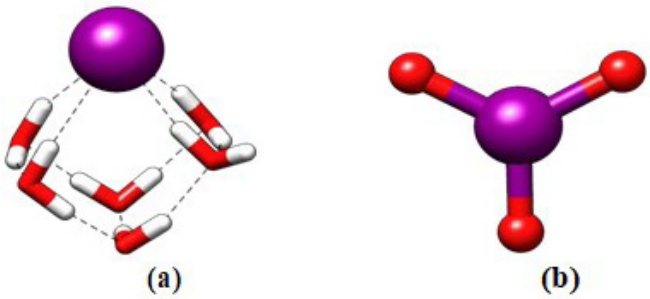

Figure 1: Optimized structures of **(a)** iodide and **(b)** iodate anion.

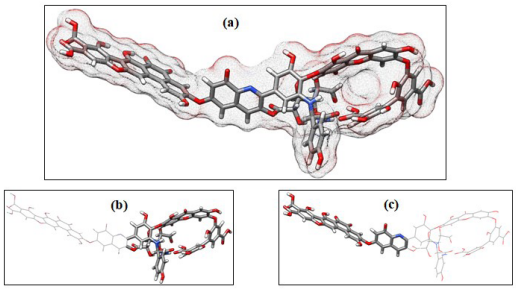

Figure 2: Optimized structure of Stevenson Humic acid. **(a)** Molecular surface map of HA species, **(b)** Head portion and **(c)** Tail portion is shown in sticks.

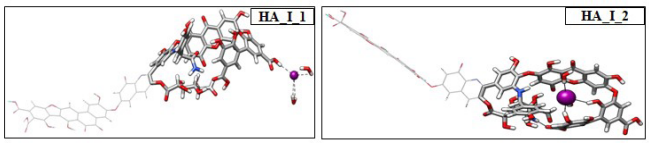

Figure 3: Optimized structures of iodide ion in head and in the tail portion.

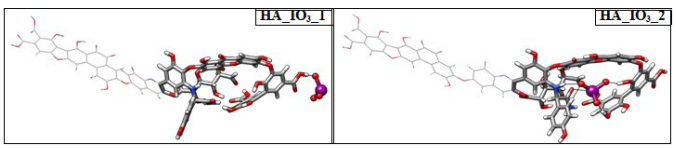

Figure 4: Optimized structures of iodate ion in head and in the tail portion.

Through AIM analysis the nonbonding interactions are identified. Both Iodide and iodate form various non-bonding interactions with host HA. It may also be noted that ρ(r) values are higher for the H-bonds formed by iodate than iodide. Therefore iodates have more affinity to bind with HA than iodide. This is in line with computed binding energy order. Our electronic structure calculations reveal that binding of iodide and iodate species are found mostly at the macrocylic type environment. Between the two iodine species, iodate binding affinities are much larger than iodide anion. Further, as the binding is largely through hydrogen bonding, we believe that pH of the medium plays a major role. The binding affinity of iodate is extremely large and the binding is dictated by both hydrogen bonding and by van der Waals interactions. Further, the macrocyclic cavity of HA perfectly fits the larger iodate anion compared to iodide. These variations lead to the stronger binding of iodate to HA, whereas the iodide anion is loosely bound. Thus, changing the pH of the HA medium should affect the binding affinities of iodide, whereas iodate is less susceptible to pH change resistant.

Table 1: QTAIM topological parameters (in a.u.), distances (in Å) for iodate and iodide species with HA in HA_IO_3_2 and HA_I_2 models.

S. No.	Bond	distance	$\rho(r)$	$\nabla^2\rho(r)$
HA_I_2				
1.	O–H···O	1.87	0.0307	0.1004
2.	O–H···O	2.11	0.0192	0.0614
3.	C–H···O	2.24	0.0166	0.0405
4.	O–H···O	2.41	0.0112	0.0417
5.	I···H	2.52	0.0216	0.0369
6.	I···H	2.59	0.0200	0.0362
7.	I···H	2.63	0.0168	0.0329
8.	I···H	2.79	0.0126	0.0266
9.	I···H	2.87	0.0118	0.0260
10.	C–H···O	2.92	0.0041	0.0159
11.	C···O	3.08	0.0069	0.0269
12.	C···I	3.40	0.0118	0.0340
13.	C···I	3.52	0.0095	0.0241
14.	C···I	3.75	0.0062	0.0167
15.	O···I	3.92	0.0038	0.0115
HA_IO_3_2				
1.	O–H···O	1.43	0.0912	0.1162
2.	O–H···O	1.49	0.0731	0.1595
3.	N–H···O	2.06	0.0208	0.0597
4.	C–H···O	2.29	0.0154	0.0407
5.	C···O	2.84	0.0119	0.0443
6.	C···O	2.88	0.0108	0.0412
7.	O···I	2.96	0.0181	0.0591
8.	C···I	3.36	0.0119	0.0326

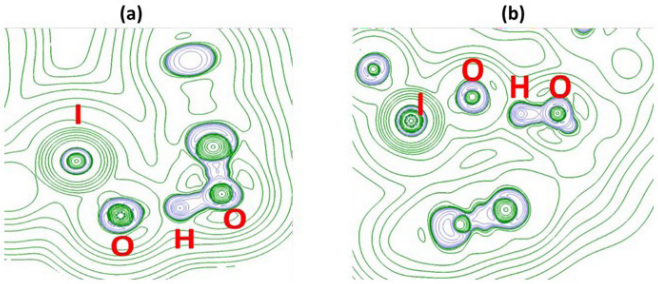

Figure 5: The Laplacian of electron density explaining the H-bonds (a.1.43 Å, b. 1.49 Å) in HA_IO_3_2.

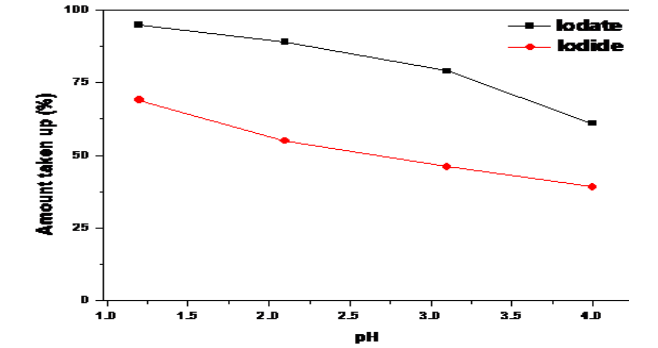

Figure 6: Sorption of iodide and iodate with HA in different pH.

We will see that our experimental studies clearly support our modeling studies (*vide infra*)

Experimental Proof

In this study, all the experimental parameters like initial concentration, equilibration time and sorbent amount were constant while varying the pH of the solution in range of 1-4. This approach could help to get an understanding of the sorption mechanism of iodine species to HA. An increase in pH is seen to reduce the sorption efficiency of humic acid for both iodide and iodate as shown in Figure 6. For instance, the sorption of iodate and iodide are more than 90% and 70% at pH~1 to 1.5, whereas at pH=4, the sorption decreases to 75% and 40% respectively. This is attributed to the fact that with increasing pH, the surface charge of humic acid becomes more negative making it less suited for sorption of anionic species. Hence there is a decrease in the sorption of both iodide and iodate anions. However it is seen that the decrease is more drastic in the case of iodide as compared to iodate. This could be attributed to the fact that iodide sorption is weak as indicated from its binding energies, while iodate sorption is strongest with HA.

Conclusions

The speciation of iodide and iodate in geochemical environments are extremely challenging but mandatory to investigate due to its environmental importance. In this work, we have carried out the geo-speciation of two important iodine species namely iodide and iodate anions. Both ions are mono-anionic, whose oxidation states are –I and +VII for iodide and iodate ions respectively. In addition, the size of the iodate ions is much larger compared to iodide ions.

The differential binding of iodide and iodate to HA be jointly investigated with detailed electronic structure calculations and experimental sorption studies. Our studies clearly reveal that iodate binding to HA is stronger compared to that of iodide ion in line with the our experimental sorption studies and those of earlier studies by Humphrey et al. [39] Further, we report that iodate binding is less susceptible on pH variations, whereas iodide binding is more sensitive to pH of HA. Our modelling studies explain the less susceptibility to pH variations in iodate binding is due to its strong binding in the macrocyclic cavity of HA.

Author Statements

Acknowledgements

MS thank BARC super-computing facilities.

Supporting Information

QTAIM topological parameters and molecular graphs of iodide and iodate bound to HA.

References

1. Rowinski MK, White TJ, Zhao J. Small and medium sized reactors (SMR): a review of technology. Renew Sustain Energy Rev. 2015; 44: 643-56.

2. Högberg L. Root causes and impacts of severe accidents at large nuclear power plants. Ambio. 2013; 42: 267-84.

3. Zablotska LB. 30 years after the Chernobyl nuclear accident: time for reflection and re-evaluation of current disaster preparedness plans. J Urban Health. 2016; 93: 407-13.

4. Tanaka S. Accident at the Fukushima di-ichi nuclear power stations of TEPCO-outline & lessons learned. Proc Jpn Acad Ser B Phys Biol Sci. 2012; 88: 471-84.

5. Ehrhardt Jr JD, Gulec S. A review of the history of radioactive iodine theranostics: the origin of nuclear ontology, mol. Imaging Radionucl Ther. 2020; 29: 88-97.

6. Hou X, Povinec PP, Zhang L, Shi K, Biddulph D, Chang CC et al. Iodine-129 in seawater offshore Fukushima: distribution, inorganic speciation, sources, and budget, Envion. Environ Sci Tech-

nol. 2013; 47: 3091-8.

7. Kenyon JA Buesseler, Casacuberta N, Castrillejo M, Otosaka S, Masqué O, et al. Distribution and Evolution of Fukushima Daiichi derived 137Cs, 90Sr, and 129I in Surface Seawater off the Coast of Japan, Environ. Sci. Technol. 2020; 54: 15066-15075.

8. McCready VR. Radioiodine – the success story in nuclear medicine. Eur J Nucl Med Mol Imaging. 2017; 44: 179-82.

9. Toyoma C, Murumatsu Y, Igarashi Y, Aoyama M, Matsuzaki H. Atmospheric fallout of 129I in Japan before the Fukushima accident: regional and global contributions (1963-2005). Environ Sci Technol. 2015; 49: 6691-700.

10. Vanmiddlesworth L, Handle J, Johns P. Iodine-129 in thyroid glands: A sensitive biological marker of fission product exposure. J Radioanal Nucl Chem. 2000; 243: 467-72.

11. Sadhu B, Sundararajan M, Bandyopadhyay T. Water-Mediated Differential binding of strontium and cesium cations in fulvic Acid. J Phys Chem B. 2015; 119: 10989-97.

12. Sundararajan M, Rajaraman G, Ghosh SK. Speciation of uranyl Ion in Fulvic Acid and Humic Acid: a DFT exploration. Phys Chem Chem Phys. 2011; 13: 18038-46.

13. Kaplan DI, Xu C, Li D, Lin P, Xing W, Nichols R, et al. Geochem. 2019; 103: 15-22.

14. Hu Q, Moran JE, Blackwood V. Geochemical cycling of iodine species in soils, UCRL book – 234137; 2007.

15. Liu W, Hu JD, Yang HX. Stabilities of iodide and iodate for iodine speciation analysis in soils. Geochem Explor Environ Anal. 2019; 19: 39-45.

16. Santschi PH, Xu C, Zhang S, Schwehr KA, Grandbois R, Kaplan DI et al. Iodine and plutonium association with natural organic matter: a review of recent advances. Geochem. 2017; 85: 121-7.

17. Hou X, Hansen V, Aldahan A, Possnert G, Lind OC, Lujaniene G. A review on speciation of iodine-129 in the environmental and biological samples. Anal Chim Acta. 2009; 632: 181-96.

18. Bowley HE, Young SD, Ander EL, Crout NMJ, Watts MJ, Bailey EH. Iodine binding to Humic Acid. Chemosphere. 2016; 157: 208-14.

19. Calais J-L. Density-functional theory of atoms and molecules. R.G. Parr and W. Yang, Oxford University Press, New York, Oxford, 1989. IX + 333 pp. Price £45.00. Int J Quantum Chem. 1993; 47: 101.

20. Turbomole. a development of University of Karlsruhe and Forschungszentrum Karlsruhe GmbH. p. 1989-2015, TURBOMOLE GmBH, since. 2007; 7.

21. Becke AD. Density-functional exchange-energy approximation with correct asymptotic behavior. Phys Rev A Gen Phys. 1988; 38: 3098-100.

22. Becke AD. Density-functional thermochemistry. III. The role of exact exchange. J Chem Phys. 1993; 98: 5648-52.

23. Grimme S, Antony J, Ehrlich S, Krieg H. A consistent and accurate ab initio parametrization of density functional dispersion correction (DFT-D) for the 94 elements H-Pu. J Chem Phys. 2010; 132: 154104.

24. Grimme S, Ehrlich S, Goerigk L. Effect of damping function in dispersion corrected density functional theory. J Comput Chem. 2011; 32: 1456-65.

25. Weigend F, Ahlrichs R. Balanced basis sets of split valence, triple zeta valence and quadruple zeta valence quantity for H to Rn: design and assessment of accuracy. Phys Chem Chem Phys. 2005; 7: 3297-305.

26. Khungar B, Roy A, Kumar A, Sadhu B, Sundararajan M. Predicting the Redox Properties of uranyl (VI/V) complexes using electronic structure calculations. Int J Quantum Chem. 2017; 117: e25370.

27. Sundararajan M. Redox potentials of uranyl ions in macrocyclic complexes: quantifying the role of counter-ions. ACS Omega. 2023; 8: 18041-6.

28. Pettersen EF, Goddard TD, Huang CC, Couch GS, Greenblatt DM, Meng EC et al. Chimera – A visualization system for exploratory research and analysis. J Comput Chem. 2004; 25: 1605-12.

29. AIM. Overland Park, KS; 2019. All. version 19.10.12, Todd A. Keith, TK Gristmill Software. Available from: aim.tkgristmill.com.

30. Bader RFW, Path AB. A Bond Path: A universal indicator of bonded interactions. J Phys Chem A. 1998; 102: 7314-23.

31. Lee C, Yang W, Parr RG. Development of the Colle-Salvetti correlation-energy formula into a functional of the electron density. Phys Rev B Condens Matter. 1988; 37: 785-9.

32. Sundararajan M, Vijay Solomon R, Ghosh SK. Elucidating the Structures and Binding of Halide ions bound to Cucurbit[6]uril, hemi- Cucurbit[6]uril and Bambus[6]uril using Density Functional Theory Calculations. Ghosh Venuvanalingam, P. RSC Adv. 2011; 1: 1333.

33. Senthilnathan D, Vijay Solomon R, Kiruthika S, Venuvanalingam P, Sundararajan M. Are cucurbiturils better capsules for bent metallocenes towards drug delivery? J Biol Inorg Chem JBIC Publ Soc Biol Inorg Chem. 2018; 23: 413-23.

34. Rasu A, Sundararajan M, Venuvanalingam P. The role of anagostic interactions in the Pd−Superoxo formation in aerobic Pd catalysed C−C coupling reaction: what do DFT computations reveal? Theoret. Comput Chem. 2023; 1228: 114284.

35. Ramkumar J, Majeed J, Chandramouleeswaran S. Insight to sorption mechanism employing nanocomposite: case study of toxic species removal. Micropor Mesopor Mater. 2021; 314: 110858.

36. Narayana B, Pasha C, Cherian T, Mathew M. Bull Chem Soc Ethiop. 2006; 20: 143-7.

37. Sadhu B, Sundararajan M, Bandyopadhyay T. Water-mediated differential binding of strontium and cesium cations in fulvic Acid. J Phys Chem B. 2015; 119: 10989-97.

38. Sadhu B, Sundararajan M, Velmurugan G, Venuvanalingam P. Elucidating the structures and cooperative binding mechanism of cesium salts to multitopic ion-pair receptor through density functional theory calculations. Dalton Trans. 2015; 44: 15450-62.

39. Humphrey OS, Young SD, Crout NMJ, Bailey EH, Ander EL, Watts MJ. Short-term iodine dynamics in soil solution. Environ Sci Technol. 2020; 54: 1443-50.

Supplementary Figures

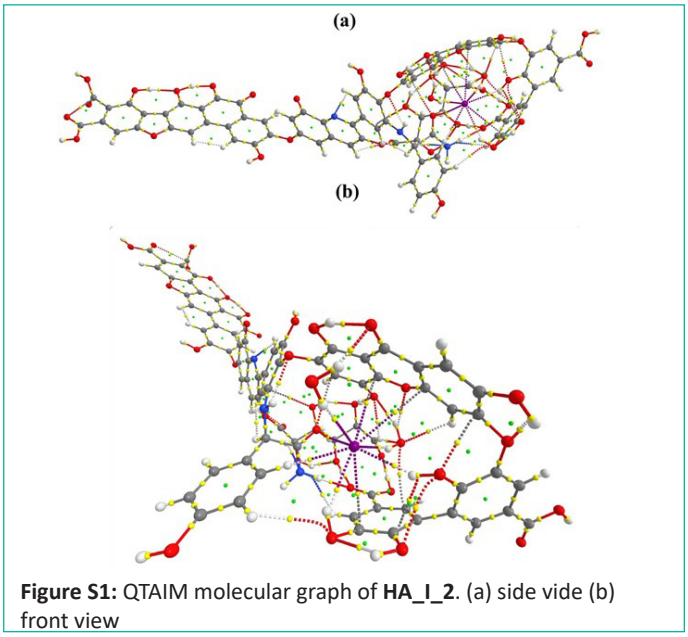

Figure S1: QTAIM molecular graph of **HA_I_2**. (a) side vide (b) front view

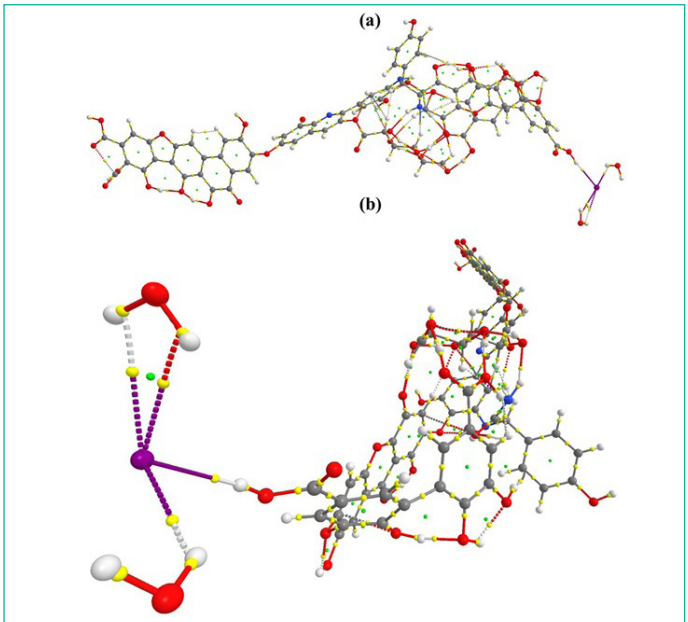

Figure S2: QTAIM molecular graph of **HA_I_1**. (a) side vide (b) front view

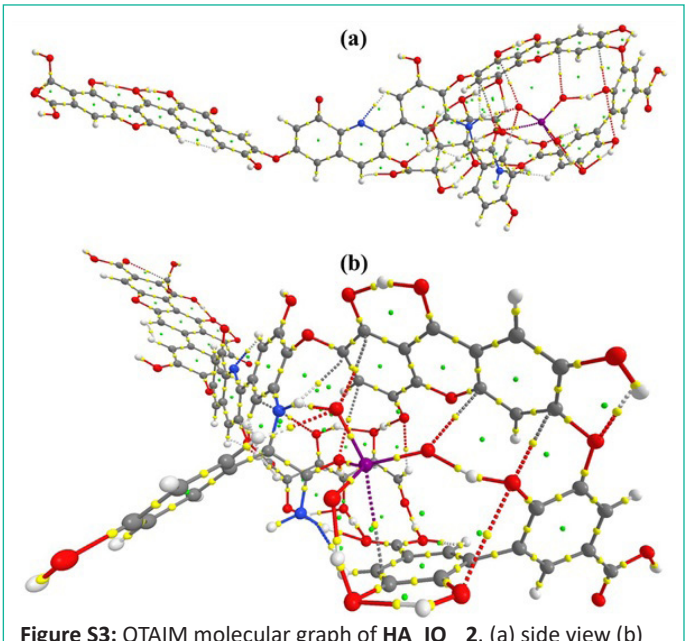

Figure S3: QTAIM molecular graph of **HA_IO_3_2**. (a) side view (b) front view

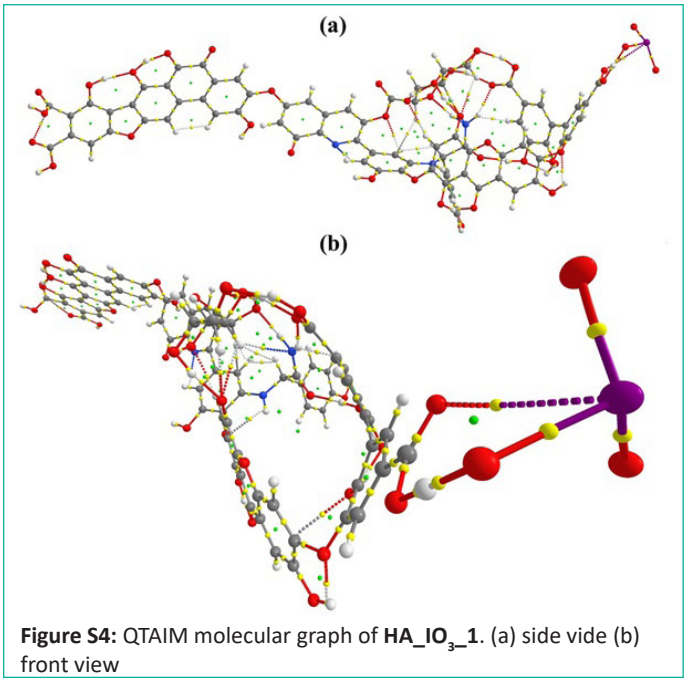

Figure S4: QTAIM molecular graph of **HA_IO_3_1**. (a) side vide (b) front view

Supplementary Table

Table S1: QTAIM topological parameters of HA_I_1 and HA_IO_3_1 (in a.u.).

S. No.	Bond	distance	$\rho(r)$	$\nabla^2\rho(r)$
HA_I_1				
1.	H···I	2.416	0.0261	0.0395
HA_IO_3_1				
1.	H···O	1.375	0.1039	0.0589
2.	O···I	3.265	0.0092	0.0336